nature physics

ARTICLES

PUBLISHED ONLINE: 22 DECEMBER 2014 | DOI: 10.1038/NPHYS3197

Experimental test of the quantum Jarzynski equality with a trapped-ion system

Shuoming An[1], Jing-Ning Zhang[1], Mark Um[1], Dingshun Lv[1], Yao Lu[1], Junhua Zhang[1], Zhang-Qi Yin[1], H. T. Quan[2,3]* and Kihwan Kim[1]*

The Jarzynski equality relates the free-energy difference between two equilibrium states to the work done on a system through far-from-equilibrium processes—a milestone that builds on the pioneering work of Clausius and Kelvin. Although experimental tests of the equality have been performed in the classical regime, the quantum Jarzynski equality has not yet been fully verified owing to experimental challenges in measuring work and work distributions in a quantum system. Here, we report an experimental test of the quantum Jarzynski equality with a single $^{171}Yb^{+}$ ion trapped in a harmonic potential. We perform projective measurements to obtain phonon distributions of the initial thermal state. We then apply a laser-induced force to the projected energy eigenstate and find transition probabilities to final energy eigenstates after the work is done. By varying the speed with which we apply the force from the equilibrium to the far-from-equilibrium regime, we verify the quantum Jarzynski equality in an isolated system.

There is increasing interest in non-equilibrium dynamics at the microscopic scale, crossing over quantum physics, thermodynamics and information theory as the experimental control and technology at such a scale have been developing rapidly. Most of the principles in non-equilibrium processes are represented in the form of inequalities, as seen in the example of the maximum work principle, $\langle W\rangle - \Delta F \geq 0$, where the average work $\langle W\rangle$ is equal to the free-energy difference ΔF only in the case of the equilibrium process. In close-to-equilibrium processes, the fluctuation–dissipation theorem is valid and connects the average dissipated energy $\langle W_{\rm diss}\rangle \equiv \langle W - \Delta F\rangle$ and the fluctuation of the system $\sigma^2/2k_{\rm B}T$. Here σ is the standard deviation of the work distribution, T is the initial temperature of the system in thermal equilibrium and $k_{\rm B}$ is the Boltzmann constant. Beyond the near-equilibrium regime, no exact results were known until Jarzynski found a remarkable equality[1] that relates the free-energy difference to the exponential average of the work done on the system:

$$\ln\left\langle e^{-W_{\rm diss}/k_{\rm B}T}\right\rangle = 0 \qquad (1)$$

The Jarzynski equality (1) is satisfied irrespective of the protocols of varying parameters of the system even when the driving is arbitrarily far from equilibrium. The relation enables us to experimentally determine ΔF of a system by repeatedly performing work at any speed. Experimental tests of the classical Jarzynski equality and its relation to the Crooks fluctuation theorem[2] have been successfully performed in various systems[3–12].

In classical systems, work can be obtained by measuring the force and the displacement, and then integrating the force over the displacement during the driving process. In the quantum regime, however, as a result of Heisenberg's uncertainty principle, we cannot determine the position and the momentum simultaneously—thus invalidating the concepts of force and displacement. Instead of measuring these classical observables, it is necessary to carry out projective measurements over the energy eigenstates to determine the work done in each realization and the work distribution[13]. With this understanding of work in quantum mechanics, the Jarzynski equality has been extended to the quantum regime[14–16] with simplicity and elegance for isolated systems, although the meaning of work and heat in open quantum systems is still not fully settled[17]. Although the theoretical derivation of the quantum Jarzynski equality is unequivocal, similar to its classical counterpart, experimental verification in a variety of systems under a range of conditions would put it on a solid experimental foundation. For this reason, experimental testing of the quantum Jarzynski equality has been a long-sought goal for many physicists[18–24]. However, even for an isolated quantum system, experimental verification has been constrained by the technical challenges in controlling quantum systems precisely and performing projective measurements to obtain the work distribution[18–21]. There have been theoretical efforts to get around such difficulties by measuring the characteristic function and then reconstructing the work distribution[22–24]. An experimental demonstration has appeared following those proposals[21]. Nevertheless, a standard way[20] of verifying the quantum Jarzynski equality by direct measurement of the work distribution is still lacking. Here, we adopt the method of two measurements over energy eigenstates and obtain the work distribution. From the work distribution, we verify the quantum Jarzynski equality.

In our experiment, we employ a trapped atomic $^{171}Yb^{+}$ ion harmonic oscillator whose Hilbert space has infinite dimensions. We implement the projective measurement on phonons[25] to determine the initial eigenstate from the thermal distribution and perform the standard phonon-distribution measurement[26–29] after work is done on the projected eigenstate. Thus, we successfully measure work and work distributions in a genuine quantum system. With these experimental techniques, we test the quantum Jarzynski equality at various initial temperatures and switching speeds. We compare the performance of the Jazynski estimate of

[1]Center for Quantum Information, Institute for Interdisciplinary Information Sciences, Tsinghua University, Beijing 100084, China. [2]School of Physics, Peking University, Beijing 100871, China. [3]Collaborative Innovation Center of Quantum Matter, Beijing 100871, China. *e-mail: htquan@pku.edu.cn; kimkihwan@mail.tsinghua.edu.cn

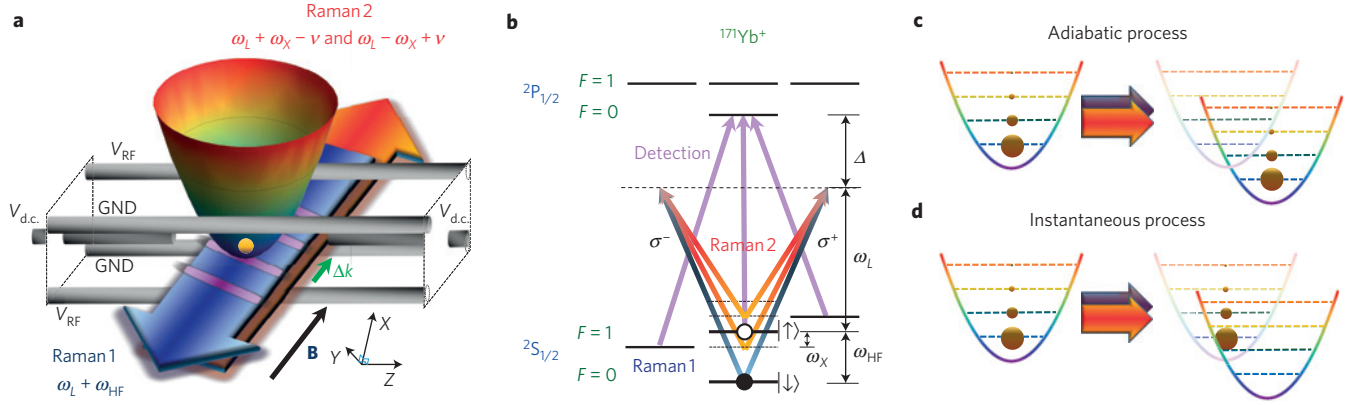

Figure 1 | Experimental set-up for testing the Jarzynski equality and equilibrium and non-equilibrium work processes. a, Schematic of the ion-trap apparatus as an ideal harmonic oscillator and the geometry of laser beams that generate an effective moving standing wave that pushes the ion. The counter propagating laser beams drive transitions between states in the $^{171}Yb^+$ ion. The frequencies of ω_L, ω_{HF}, and ω_X are shown in **b**. **b**, The basic level structure of the $^{171}Yb^+$ ion and the relevant laser frequencies. The Raman laser beams introduce a state-dependent force. When their beat-note frequencies are adjusted to near $\omega_{HF} \pm \omega_X$, the force pushes the ion along the $\pm\Delta k$ direction for the $(|\uparrow\rangle \pm |\downarrow\rangle)/\sqrt{2}$ state of the ion. **c**, For the perfect adiabatic process the phonon distributions before and after are unchanged. **d**, For the non-equilibrium process, the final phonon states are widely distributed. In the case of both adiabatic and instantaneous shifts of the harmonic oscillator, the Jarzynski equality should be valid, as long as the system is initially prepared in a thermal equilibrium state.

ΔF to that obtained using the average work and the fluctuation–dissipation theorem.

Ion-trap systems have shown a high degree of control in the quantum regime[27]. Controls of the harmonic oscillator are performed through coupling to the two electronic levels (qubit) of the $^{171}Yb^+$ ion in the $S_{1/2}$ manifold, denoted by $|F=1, m_F=0\rangle \equiv |\uparrow\rangle$ and $|F=0, m_F=0\rangle \equiv |\downarrow\rangle$, which are separated by $\omega_{HF} = (2\pi)12.642\,\text{GHz}$. As shown in Fig. 1, the $^{171}Yb^+$ ion is confined in harmonic potentials with trap frequencies $\omega_X = (2\pi)3.1\,\text{MHz}$, $\omega_Y = (2\pi)2.7\,\text{MHz}$, $\omega_Z = (2\pi)0.6\,\text{MHz}$, respectively.

We perform work on the system by applying a laser-induced force and shifting the centre of the potential in the X-direction. The force is implemented by the counter-propagating laser beams shown in Fig. 1a,b, which is equivalent to generating a so-called qubit-state-dependent force[30,31]. A pair of laser beams with frequency differences of $\omega_\pm = \omega_{HF} \pm (\omega_X - \nu)$ produce the following Hamiltonian in the rotating frame about $H_0 = (1/2)\hbar\omega_{HF}\hat{\sigma}_z + \hbar(\omega_X - \nu)\left(\hat{a}^\dagger\hat{a} + (1/2)\right)$, where $\hat{a}^\dagger$ and $\hat{a}$ are the creation and the annihilation operators acting on phonons, after taking the rotating-wave approximation,

$$H(t) = \frac{\hat{P}^2}{2M_e} + \frac{1}{2}M_e\nu^2\hat{X}^2 + f(t)\hat{X}\hat{\sigma}_x \qquad (2)$$

Here, $\hat{P} = i\sqrt{\frac{\hbar M_e\nu}{2}}(\hat{a}^\dagger - \hat{a})$ and $\hat{X} = \sqrt{\frac{\hbar}{2M_e\nu}}(\hat{a}^\dagger + \hat{a})$ are momentum and position operators, $M_e = (\omega_X/\nu)M$ is the scaled mass of the $^{171}Yb^+$ mass, M, $\nu(\equiv\omega_X \pm(\omega_{HF} - \omega_\pm)) = (2\pi)20.0\,\text{kHz}$ is the effective trap frequency, $f(t) = (1/2)\hbar\Delta k\Omega(t)$ is the effective force, $\hat{\sigma}_x$ is the Pauli operator, Δk is the net wavevector of the counter-propagating laser beams along the X-axis and the Rabi frequency, Ω, is proportional to the intensity of the laser beams.

The force shifts the trap centre by $-f(t)/M_e\nu^2$ and reduces the ground-state energy by $f^2(t)/2M_e\nu^2$. In our experiment, the maximum force is 4.16 zN ($\times 10^{-21}$N), produced by the maximum Rabi frequency $\Omega_{max} = (2\pi)378\,\text{kHz}$, which shifts the centre position by 5.6 nm. When we adiabatically add the force $f(t)$ to the maximum value, the final state distribution is conserved in the new basis and still in thermal equilibrium, as shown Fig. 1c. In contrast, if we increase the force to the same value instantaneously, the final states are highly excited, which represents a far-from-equilibrium process and is shown in Fig. 1d. In both cases, we would measure the same average of the exponentiated dissipated work $\langle \exp(-W_{diss}/k_BT)\rangle$, which is used to test the Jarzynski equality.

For the time-dependent quantum system $H(t)$ (2), where the eigenvalues and the eigenstates are denoted by $E_n(t)$ and $|n(t)\rangle$, the phonon number state, the work done on the system from $t=0$ to $t=\tau$ is defined by $E_{\bar{n}}(\tau) - E_n(0)$. The distribution of the work is described by the following equation[13]

$$P(W) = \sum_{n,\bar{n}} \delta[W - (E_{\bar{n}}(\tau) - E_n(0))]P_{\bar{n}\leftarrow n}P_n^{th} \qquad (3)$$

where $P_n^{th} = \exp(-E_n(0)/k_BT)/\left[\sum_n \exp(-E_n(0)/k_BT)\right]$ gives the initial thermal distribution and $P_{\bar{n}\leftarrow n} = |\langle\bar{n}(\tau)|\hat{U}|n(0)\rangle|^2$ is the transition probability from the initial state $|n(0)\rangle$ to the final state $|\bar{n}(\tau)\rangle$ under the evolution operator $\hat{U}$. In testing the validity of the Jarzynski equality, it is necessary to observe that the average of the exponentiated work $\langle \exp(-W/k_BT)\rangle \equiv \sum P(W)\exp(-W/k_BT)$ is independent of the work protocol from the quasi-static to the far-from-equilibrium regime. The essential part of the experimental test in the quantum regime is to obtain the conditional probability from the projected energy eigenstate $|n(0)\rangle$ out of the thermal distribution to the final eigenstate $|\bar{n}(\tau)\rangle$ after the work is done on the projected state.

In our experiment, we follow a similar procedure to that proposed in refs 18–20, which is composed of four stages: preparation of the thermal state; projection to an energy eigenstate; application of work on the eigenstate; the measurement of the final phonon distribution.

We prepare a thermal state of the trapped ion's harmonic motion in the X-direction. We first cool the vibrational mode near to the ground state $|n=0\rangle$ by resolved-sideband cooling[32] right after the Doppler cooling. Then we allow the system to heat up to the desired temperature. The heating and thermalization of the system have been extensively studied both experimentally and theoretically[33–36]. The process is described well by the model of a harmonic oscillator coupled to a high-temperature reservoir, which follows a sequence of thermal equilibrium states[33–36]. We observe the thermal distribution at each waiting time, where the temperature increases as shown in Fig. 2a. We characterize the distribution by both the

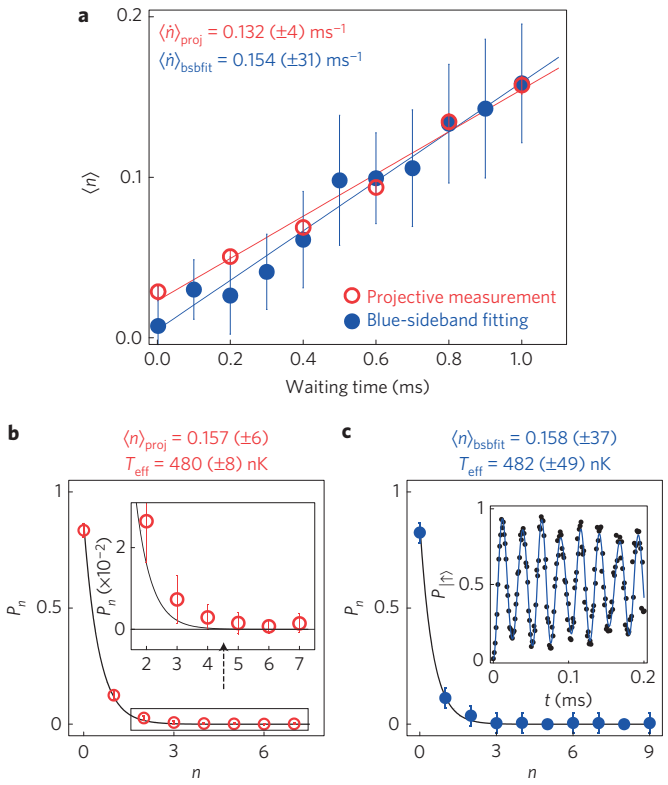

Figure 2 | Thermal state preparation of the phonon and measurement results. a, Measurements on the heating rate of the trapped ion's harmonic motion in the *X*-direction. After the ground-state cooling, the average phonon number increases linearly with the waiting time. The temperature is extracted from the average phonon number $\langle n \rangle$ using $T_{eff} = \hbar\nu/k_B \ln(1+1/\langle n \rangle)$, where ν is the effective trap frequency. Projective measurements on the phonon states (red circles) are performed at various waiting times and the results are compared against those from the phonon-distribution measurement based on the dependence of the blue-sideband Rabi frequency on the phonon number shown in equation (4) (filled blue circles). The measured heating rate given by the phonon projection is consistent within error bars with that from fitting the blue-sideband transition by equation (4). **b**, Phonon distribution (red circles) measured by projective measurement at a 1 ms waiting time, fitted using the thermal distribution function $P_n^{th} = \langle n \rangle^n/(\langle n \rangle+1)^{n+1}$ (solid line). The measurement procedure shown in Fig. 3 is repeated 5×10^6 times, where the phonon state is determined in each single run in the projective measurement. Here, the experimentally determined errors in the detection are corrected (Methods). Error bars indicate the standard deviation. **c**, Phonon distribution at 1 ms obtained by fitting the data in the inset with a superposition of Fock states (filled blue circles) and with a thermal distribution with $\langle n \rangle$ (solid line) using equation (4). Error bars represent one standard deviation in parameter estimations of the fitting. The method is applied to obtain the error bars for the remaining figures and table (for more details, see the Supplementary Information).

projective measurement and the standard fitting method using the Rabi-frequency dependence of the sideband transition on the phonon state[26–29].

Figure 2b shows the phonon distribution of a thermal state obtained by the projective measurement at 1 ms waiting time after the ground-state cooling, yielding $\langle n \rangle = 0.157(\pm 6)$, $T_{eff} = 480(\pm 8)$ nK. The temperature is extracted from the average phonon number $\langle n \rangle$ using $T_{eff} = \hbar\nu/[k_B \ln(1+1/\langle n \rangle)]$, where the effective frequency of the harmonic oscillator ν is different from the real motional frequency ω_X. We use the thermal state at 1 ms as well as 0.3 ms ($\langle n \rangle = 0.051(\pm 2)$, $T_{eff} = 316(\pm 4)$ nK) and 0.6 ms ($\langle n \rangle = 0.094(\pm 4)$, $T_{eff} = 390(\pm 6)$ nK) to start with different initial temperatures for the test of the Jarzynski equality. We finally determine the population of each eigenstate by fitting with the thermal distribution, owing to the limited precision of the projective measurement below the 10^{-3} level (see Methods and Supplementary Information). The resulting phonon distribution from the projective measurement is consistent with that from the fitting method, as shown in Fig. 2c. Note that in the fitting method we cannot decide the phonon state in a single measurement nor carry out successive operations on the projected Fock state.

Our projective measurement is composed of two parts: first, find the projected energy eigenstate $|n\rangle$ and then deterministically generate the same phonon Fock state. The projected state is determined by repeating the sequence of phonon subtraction and qubit state detection and counting the number of repetitions until the first fluorescence is observed (Fig. 3a). If the fluorescence is detected at the $(n+1)$th iteration for the first time, the projected state is $|n\rangle$ (Fig. 3b)[25].

The phonon subtraction ($|n\rangle \rightarrow |n-1\rangle$, shown in Fig. 3c) is performed by the successive application of the π pulse of the resonant carrier transition ($|\downarrow,n\rangle \rightarrow |\uparrow,n\rangle$) and the adiabatic blue-sideband transition ($|\uparrow,n\rangle \rightarrow |\downarrow,n-1\rangle$). We apply the scheme of the adiabatic spin-flip operation in ref. 37 to the phonon system, where a near-perfect transition from $|\uparrow,n\rangle$ to $|\downarrow,n-1\rangle$ with the same duration is achieved regardless of the phonon number n (see Methods and Supplementary Information). After the phonon subtraction, only the state $|\downarrow,0\rangle$ is transferred to the bright $|\uparrow\rangle$ state that scatters photons at the qubit-detection sequence (Fig. 3e), whereas the other states remain in the dark $|\downarrow\rangle$ state with a reduction of one quanta (Fig. 3f). Therefore, the projected state $|\downarrow,n\rangle$ generates the fluorescence at the $(n+1)$th successive operation of subtraction and detection. At each waiting time, we typically perform 5×10^6 projective measurements with seven iterations of subtraction and detection. At each measurement, the projected energy eigenstate is determined. The Fock state $|n\rangle$ is deterministically prepared by n repeated applications of the π pulses of the blue-sideband and the carrier transition after another ground-state cooling[26].

Because the projection scheme has two totally independent sequences: determination and preparation, we completely separate the sequence of preparing the Fock state $|n\rangle$ from the sequence of detecting it. We prepare the initial Fock states up to $|n=5\rangle$, as the total population of Fock states $n>5$ at $\langle n \rangle = 0.157$ is less than 10^{-5} and the estimated error without these states is smaller than 10^{-3}, even for the case of the fastest driving. Figure 4a shows the fidelity in the preparation of the phonon number state up to $|n=5\rangle$. We produce the $|n\rangle$ state up to $n=5$ with over 90% fidelity (see Supplementary Information).

After determining and preparing the projected energy eigenstate $|n\rangle$, we apply work to the system. We apply the laser-induced force of equation (2) on the prepared state for durations of 5 μs, 25 μs and 45 μs with a linearly increasing strength to the same maximum value, as shown in Fig. 4b. The qubit state dependence in the Hamiltonian (2) plays no role, because the electronic state is prepared in the eigenstate of $\hat{\sigma}_x$, $(|\uparrow\rangle \pm |\downarrow\rangle)/\sqrt{2}$ (see Methods). Note that the laser-induced effective force occurs in a rotating frame. Because the effective force term does not commute with H_0, we adiabatically bring the final state to the lab frame before measurement of the final phonon distribution. We have carefully studied the adiabatic process and observed less than 0.015 change of the average phonon number when the total duration is 50 μs, including the heating effect (see Methods and the Supplementary Information).

After the work is done on the state $|n\rangle$, we measure the final distribution of phonon number states by applying the blue- and

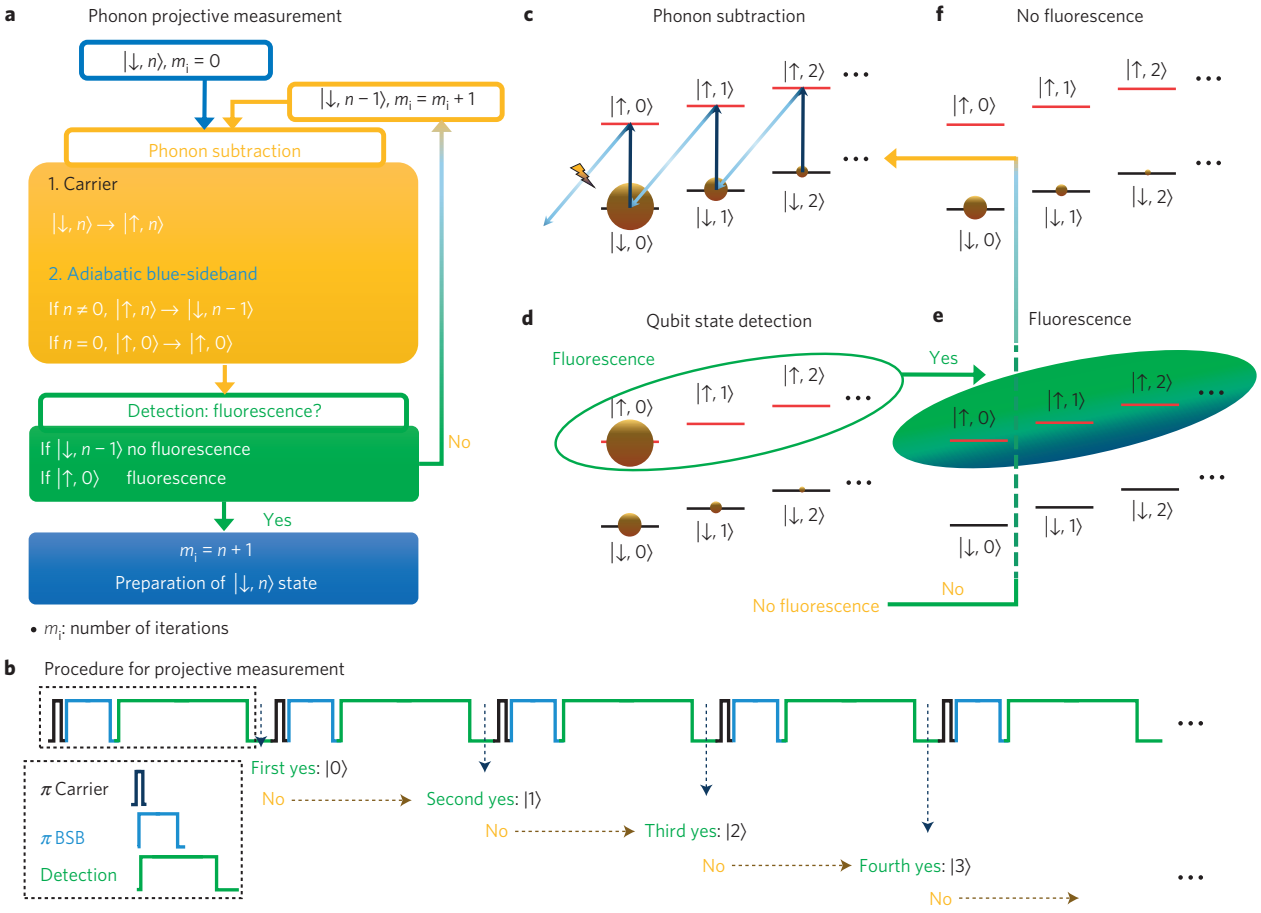

Figure 3 | Experimental scheme for the projective measurement of the phonon state. a,**b**, Flow chart and time sequence, respectively, for the projective measurement. If the first fluorescence is observed after $(n+1)$ repetitions of phonon subtraction and qubit state detection, the projected phonon state is $|n\rangle$. **c**, The phonon subtraction operation, which changes the phonon state from $|n\rangle$ to $|n-1\rangle$, is composed of the π pulses of the resonant carrier transition (black arrow) and the adiabatic blue-sideband transition (blue arrow, see also Methods). The subtraction $|n\rangle \rightarrow |n-1\rangle$ is performed for any phonon Fock state except $|n=0\rangle$, which is transferred to $|\uparrow, n=0\rangle$. **d**, Qubit state detection. **e**,**f**, On application of the detection laser beam (Fig. 1c), fluorescence is observed for the $|\uparrow\rangle$ state (**e**), which was the $|\downarrow, n=0\rangle$ state before the phonon subtraction, whereas no fluorescence is detected for the $|\downarrow\rangle$ state (**f**), where phonon states are reduced by one quanta. The state originally projected to $|\downarrow, n\rangle$ reaches the state $|\uparrow, n=0\rangle$, which shows fluorescence after $(n+1)$ repetitions of subtraction and detection (**c**,**d**) procedures.

red-sideband transitions and fitting the signals using the maximal likelihood method with the parameters of the Fock state population P_n (see Methods and Supplementary Information). We observe the time evolution of the blue- and red-sideband transitions up to 250 μs with a step size of 1 μs by averaging 200 repetitions of each step.

Figure 4c summarizes how the final phonon distributions depend on the speed at which work is applied on a Fock state $|n\rangle$, which is given by the transition probabilities $P_{\bar{n}\leftarrow n}$ in equation (3). The raw data and fitting results are presented in the Supplementary Information. Figure 4c shows that our work protocols range from the equilibrium to the non-equilibrium regime. For the slow ramp, $\tau = 45$ μs, the final distribution of the phonon states is almost identical to the initial distribution shown in Fig. 4a. For the case of the fastest ramp, $\tau = 5$ μs, it is clearly shown that the final population is most widely spread, which indicates the process is out of equilibrium.

Figure 4d shows the probability distribution of the dissipated work, $W_{\rm diss}$, constructed from the transfer probabilities $P_{\bar{n}\leftarrow n}$ shown in Fig. 4c with a phonon distribution P_n^{th} of effective temperature $T_{\rm eff} = 480$ nK ($\langle n\rangle = 0.157$). It is clear that ramping the force with a duration $\tau = 45$ μs is close to an adiabatic process, as there is almost no change in the phonon distribution in the work process. Similar to the results for the classical regime[4], the mean value and the width of the distribution of the dissipated work increase with the ramping speed. The standard deviations of the dissipated work in the two fast ramp protocols ($\tau = 5$ μs and $\tau = 25$ μs) are of the order of $k_{\rm B}T_{\rm eff}$ (refs 1,4) and negative dissipated work, as a manifestation of the microscopic 'violations' of the second law, appears clearly in the two fast ramp protocols. Note that in the classical version of our model, only a Gaussian profile of the distribution of dissipated work exists in an open system[38–40] as well as in an isolated system (see also Supplementary Information) regardless of the protocol. The non-Gaussian profile is predicted in ref. 41 at the extreme low initial temperature $\langle n\rangle < 1$, which is naturally in the quantum regime.

Table 1 summarizes the performances of the three different estimates of the change in free energy from the Jarzynski equality, the fluctuation–dissipation theorem and the mean dissipated energy. Our experimental data clearly demonstrate the validity of the Jarzynski equality when other estimates deviate from the ideal values[42]. For comparison, we apply three work protocols at three initial temperatures. The free energy differences ΔF are $-2.63\ k_{\rm B}T_{\rm eff}$ ($T_{\rm eff} = 316$ nK), $-2.13\ k_{\rm B}T_{\rm eff}$ ($T_{\rm eff} = 390$ nK) and $-1.73\ k_{\rm B}T_{\rm eff}$ ($T_{\rm eff} = 480$ nK). For the case of $\tau = 45$ μs, the average dissipated energy provides estimations of ΔF within 2σ. For the

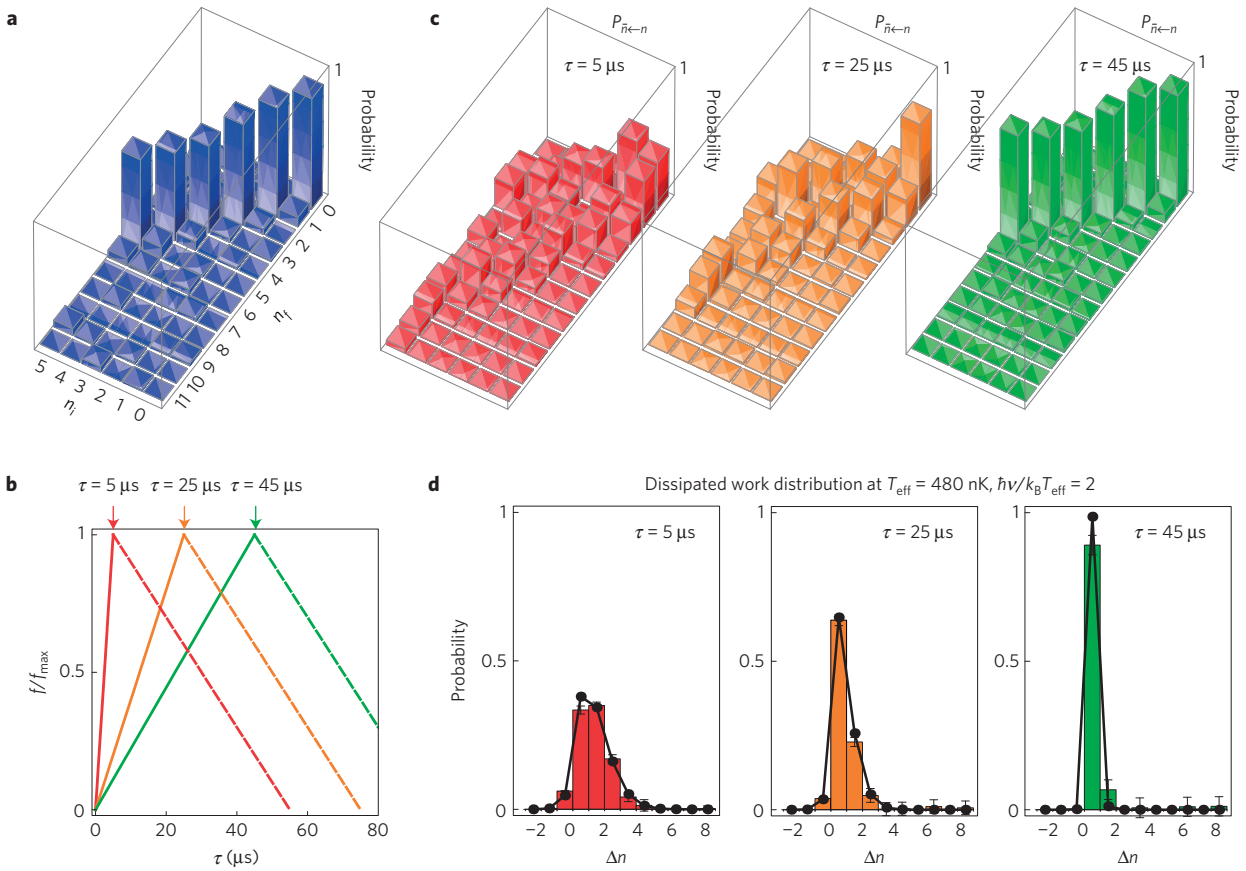

Figure 4 | Dissipated work $W_{diss} = W - \Delta F = \hbar\nu\Delta n$ and probabilities $P_{\tilde{n}\leftarrow n}$ for three different ramping speeds of the force. a, Populations of the prepared phonon Fock states from $n = 0$ to 5 (see also Supplementary Methods). **b**, The force is linearly increased to the maximum value for three different durations, corresponding to the far-from-equilibrium (5 μs), the intermediate (25 μs) and the near-adiabatic (45 μs) work processes. The dashed line shows the adiabatic process used to bring the system to the lab frame in 50 μs. **c**, Transfer probabilities from $|n(0)\rangle\langle n(0) = 0, 1, \ldots, 5)$ to $|\tilde{n}(\tau)\rangle$ at the three ramping speeds measured by the maximal-likelihood method of the blue- and red-sideband transitions after the work process (see also Supplementary Information). The time evolutions by the blue- and red-sideband transitions are monitored for up to 250 μs with a 1 μs time step by averaging 200 repetitions at each step. **d**, Distributions of the dissipated work at $\langle n\rangle = 0.157$ give full information to test the validity of the quantum Jarzynski equality given by equation (1). The data bars result from the transfer probability (**c**) and the thermal distributions by projective measurements shown in Fig. 2b. The solid lines are results from the analytical calculations. The three dissipated work distributions show the characteristics of far-from-equilibrium, intermediate and adiabatic processes, with the width increasing as the process moves away from equilibrium. The work distribution for a duration of 5 μs clearly shows a non-Gaussian profile, which has a quantum origin. For a duration of 45 μs, the distribution is close to a delta function.

Table 1 | Summary of the experimental test of the quantum Jarzynski equality and comparison with other estimates.

$\Delta F/k_B T_{eff}$	T_{eff} (nK)	$-\ln\langle e^{-W_{diss}/k_B T_{eff}}\rangle$			$\langle W_{diss}/k_B T_{eff}\rangle - 1/2(\sigma^2/(k_B T_{eff})^2)$			$\langle W_{diss}/k_B T_{eff}\rangle$		
		$\tau = 5\,\mu s$	$\tau = 25\,\mu s$	$\tau = 45\,\mu s$	$\tau = 5\,\mu s$	$\tau = 25\,\mu s$	$\tau = 45\,\mu s$	$\tau = 5\,\mu s$	$\tau = 25\,\mu s$	$\tau = 45\,\mu s$
−2.63	316	−0.032(37)	0.006(34)	0.042(52)	−1.601(443)	−0.718(568)	−0.087(154)	2.573(313)	0.929(401)	0.211(109)
−2.13	390	−0.033(35)	0.005(33)	0.037(50)	−0.889(346)	−0.426(442)	−0.027(120)	2.033(245)	0.749(313)	0.168(85)
−1.73	480	−0.034(34)	0.003(31)	0.031(48)	−0.505(269)	−0.260(342)	0.002(93)	1.598(190)	0.602(242)	0.131(66)

The experimental results at various temperatures and rates of application of the force are close to the ideal values of $-\ln\langle e^{-W_{diss}/k_B T}\rangle = 0$ within error bars, where $W_{diss} = W - \Delta F$ and the energy scale is $k_B T_{eff}$. The other estimates of the free-energy difference ΔF using the average work $\langle W_{diss}/k_B T_{eff}\rangle$ and the fluctuation–dissipation relation $\langle W_{diss}/k_B T_{eff}\rangle - 1/2(\sigma^2/(k_B T_{eff})^2)$ are compared against those from the Jarzynski equality[42]. For these estimates from experimental results, high phonon states with populations significantly smaller than the error bars are not included.

case of $\tau = 45\,\mu s$ and $\tau = 25\,\mu s$, the fluctuation–dissipation theorem provides estimations within σ and 2σ, respectively, indicating these protocols are in linear response regime. For the case of $\tau = 5\,\mu s$, the far-from-equilibrium protocol, only the Jarzyski estimate gives reasonable values of the free-energy differences. We found that the main error in the experiment comes from heating of the phonon mode during the adiabatic return, but the amount of error from heating in the Jarzynski estimate is less than the experimental uncertainty according to our numerical simulation. Detailed experimental imperfections and errors are discussed in the Supplementary Information.

For many decades, measurement of the work and its distribution in a quantum system has been only a thought experiment and this fact may explain why attempts to directly test the quantum Jarzynski equality in experiments have not been successful so far. Based on the ground-breaking technology of isolating and manipulating individual quantum systems[43,44] developed in the past three decades, we further developed the phonon projective-measurement method,

enabling us to experimentally measure the mechanical work and its distribution in a quantum system undergoing an arbitrary non-equilibrium process. Besides being used in verifying the quantum Jarzynski equality, our experimental breakthrough could be applied to make many other thought experiments in quantum thermodynamics possible in the laboratory. For example, the method can be immediately used to test Crooks' relation in the quantum regime[2,5] and in further investigations of the equality in open quantum systems[17,20]. It could also be adapted to studies of quantum heat engines[45,46] by experimentally exploring work and heat in thermodynamic cycles. Furthermore, the phonon projective measurement would be an essential tool for the boson-sampling problem[47] with phonons[25].

Methods

In the projected measurement, we transfer the $|\uparrow,n\rangle$ state to the $|\downarrow,n-1\rangle$ state in the same amount of time independent of the phonon number by adjusting the intensity and frequency of the laser beam in the form $\Omega_b(t)=\Omega_{n,n+1,\max}\sin((\pi/T)t)$ and $\delta(t)=\delta_0\cos((\pi/T)t)$ (ref. 37). The main errors in the phonon projective measurement come from two sources: imperfections in qubit state detection and heating of the phonon state during the measurement. We apply a correction method of state detection[48] to the phonon system. The phonon state changes due to the heating process are tracked and reversed by means of a calculation. We apply the $\hat{\sigma}_x$-dependent force and prepare the eigenstate of $\hat{\sigma}_x$ during application of the force and the adiabatic process back to the lab frame. We bring the phonon distribution from the rotating frame to the lab frame by linearly reducing the laser intensity in a time $T_a=(2\pi/|\nu|)$. We use the maximal-likelihood method to find the phonon distributions by fitting interference of the blue- and red-sideband transitions among different phonon modes following the methods in ref. 49. The values of P_n can be determined by observing the time evolution of the probability $P_\uparrow^{\pm}(t)$ of finding the ion in the $|\uparrow\rangle$ state during the blue(red)-sideband transitions, which is written as

$$P_\uparrow^{\pm}(t)=\frac{1}{2}\sum_n P_n\left[1-e^{-\gamma_\pm t}A_\pm\cos(2\Omega_{n,n\pm1}t)\right] \quad (4)$$

Here $P_\uparrow^{\pm}(t)$ is experimentally measured through the qubit-state-dependent fluorescence[50,51]. The decay rate $\gamma_\pm$ is included to take into account laser intensity fluctuations and heating. The contrast parameter $A_\pm$ is required to take into account imperfections in the state preparation and detection. The Supplementary Information describes the detailed experimental schemes with supporting data.

Received 16 April 2014; accepted 14 November 2014; published online 22 December 2014

References

1. Jarzynski, C. Nonequilibrium equality for free energy differences. *Phys. Rev. Lett.* **78,** 2690–2693 (1997).
2. Crooks, G. E. Entropy production fluctuation theorem and the nonequilibrium work relation for free-energy differences. *Phys. Rev. E* **60,** 2721–2726 (1999).
3. Hummer, G. & Szabo, A. Free energy reconstruction from nonequilibrium single-molecule pulling experiments. *Proc. Natl Acad. Sci. USA* **98,** 3658–3661 (2001).
4. Liphardt, J., Dumont, S., Smith, S. B., Tinoco, I. J. & Bustamante, C. Equilibrium information from nonequilibrium measurements in an experimental test of the Jarzynski equality. *Science* **296,** 1832–1835 (2002).
5. Collin, D. *et al.* Verification of the Crooks fluctuation theorem and recovery of RNA folding free energies. *Nature* **437,** 231–234 (2005).
6. Douarche, F., Ciliberto, S., Petrosyan, A. & Rabbiosi, I. An experimental test of the Jarzynski equality in a mechanical experiment. *Europhys. Lett.* **70,** 593–599 (2005).
7. Bustamante, C., Liphardt, J. & Ritort, F. The nonequilibrium thermodynamics of small systems. *Phys. Today* **58,** 43–48 (July, 2005).
8. Blickle, V., Speck, T., Helden, L., Seifert, U. & Bechinger, C. Thermodynamics of a colloidal particle in a time-dependent nonharmonic potential. *Phys. Rev. Lett.* **96,** 070603 (2006).
9. Harris, N. C., Song, Y. & Kiang, C-H. Experimental free energy surface reconstruction from single-molecule force spectroscopy using Jarzynski's equality. *Phys. Rev. Lett.* **99,** 068101 (2007).
10. Saira, O-P. *et al.* Test of the Jarzynski and Crooks fluctuation relations in an electronic system. *Phys. Rev. Lett.* **109,** 180601 (2012).
11. Jarzynski, C. Equalities and inequalities: Irreversibility and the second law of thermodynamics at the nanoscale. *Annu. Rev. Condens. Matter Phys.* **2,** 329–351 (2011).
12. Seifert, U. Stochastic thermodynamics, fluctuation theorems and molecular machines. *Rep. Prog. Phys.* **75,** 126001 (2012).
13. Talkner, P., Lutz, E. & Hänggi, P. Fluctuation theorems: Work is not an observable. *Phys. Rev. E* **75,** 050102(R) (2007).
14. Tasaki, H. Jarzynski relations for quantum systems and some applications. Preprint at http://arXiv.org/abs/cond-mat/0009244 (2000).
15. Kurchan, J. A quantum fluctuation theorem. Preprint at http://arXiv.org/abs/cond-mat/0007360 (2000).
16. Mukamel, S. Quantum extension of the Jarzynski relation: Analogy with stochastic dephasing. *Phys. Rev. Lett.* **90,** 170604 (2003).
17. Esposito, M., Harbola, U. & Mukamel, S. Nonequilibrium fluctuations, fluctuation theorems, and counting statistics in quantum systems. *Rev. Mod. Phys.* **81,** 1665–1702 (2009).
18. Huber, G., Schmidt-Kaler, F., Deffner, S. & Lutz, E. Employing trapped cold ions to verify the quantum Jarzynzki equality. *Phys. Rev. Lett.* **101,** 070403 (2008).
19. Huber, G. T. *Quantum Thermodynamics with Trapped Ions* PhD thesis, Univ. Ulm (2010).
20. Campisi, M., Hänggi, P. & Talkner, P. Colloquium: Quantum fluctuation relations: Foundations and applications. *Rev. Mod. Phys.* **83,** 771–791 (2011).
21. Batalhao, T. *et al.* Experimental reconstruction of work distribution and verification of fluctuation relations at the full quantum level. *Phys. Rev. Lett.* **113,** 140601 (2014).
22. Heyl, M. & Kehrein, S. Crooks relation in optical spectra: Universality in work distributions for weak local quenches. *Phys. Rev. Lett.* **108,** 190601 (2012).
23. Dorner, R. *et al.* Extracting quantum work statistics and fluctuation theorems by single qubit interferometry. *Phys. Rev. Lett.* **110,** 230601 (2013).
24. Mazzola, L., Chiara, G. D. & Paternostro, M. Measuring the characteristic function of the work distribution. *Phys. Rev. Lett.* **110,** 230602 (2013).
25. Shen, C., Zhang, Z. & Duan, L-M. Scalable implementation of boson sampling with trapped ions. *Phys. Rev. Lett.* **112,** 050504 (2014).
26. Meekhof, D., Monroe, C., King, B., Itano, W. & Wineland, D. Generation of nonclassical motional states of a trapped atom. *Phys. Rev. Lett.* **76,** 1796–1799 (1996).
27. Leibfried, D., Blatt, R., Monroe, C. & Wineland, D. Quantum dynamics of single trapped ions. *Rev. Mod. Phys.* **75,** 281–324 (2003).
28. Walther, A. *et al.* Controlling fast transport of cold trapped ions. *Phys. Rev. Lett.* **109,** 080501 (2012).
29. Bowler, R. *et al.* Coherent diabatic ion transport and separation in a multizone trap array. *Phys. Rev. Lett.* **109,** 080502 (2012).
30. Haljan, P. C., Brickman, K-A., Deslauriers, L., Lee, P. J. & Monroe, C. Spin-dependent forces on trapped ions for phase-stable quantum gates and entangled states of spin and motion. *Phys. Rev. Lett.* **94,** 153602 (2005).
31. Lee, P. J. *et al.* Phase control of trapped ion quantum gates. *J. Opt. B* **7,** S371–S383 (2005).
32. Monroe, C. *et al.* Resolved-sideband Raman cooling of a bound atom to the 3d zero-point energy. *Phys. Rev. Lett.* **75,** 4011–4014 (1995).
33. Turchette, Q. A. *et al.* Heating of trapped ions from the quantum ground state. *Phys. Rev. A* **61,** 063418 (2000).
34. Turchette, Q. *et al.* Decoherence and decay of motional quantum states of a trapped atom coupled to engineered reservoirs. *Phys. Rev. A* **62,** 053807 (2000).
35. Myatt, C. J. *et al.* Decoherence of quantum superpositions through coupling to engineered reservoirs. *Nature* **403,** 269–273 (2000).
36. Intravaia, F., Maniscalcoa, S., Piilob, J. & Messina, A. Quantum theory of heating of a single trapped ion. *Phys. Lett. A* **308,** 6–10 (2003).
37. Zhang, J., Zhang, J., Zhang, X. & Kim, K. Realization of geometric Landau–Zener–Stückelberg interferometry. *Phys. Rev. A* **89,** 013608 (2014).
38. Mazonka, O. & Jarzynski, C. Exactly solvable model illustrating far-from-equilibrium predictions. Preprint at http://arXiv.org/abs/cond-mat/9912121 (1999).
39. Speck, T. & Seifert, U. Distribution of work in isothermal nonequilibrium processes. *Phys. Rev. E* **70,** 066112 (2004).
40. Imparato, A., Peliti, L., Pesce, G., Rusciano, G. & Sasso, A. Work and heat probability distribution of an optically driven Brownian particle: Theory and experiments. *Phys. Rev. E* **76,** 050101(R) (2007).
41. Talkner, P., Burada, P. S. & Hänggi, P. Statistics of work performed on a forced quantum oscillator. *Phys. Rev. E* **78,** 011115 (2008).
42. Hendrix, D. A. & Jarzynski, C. A "fast growth" method of computing free energy differences. *J. Chem. Phys.* **114,** 5974–5981 (2001).
43. Wineland, D. Nobel Lecture: Superposition, entanglement, and raising Schrodinger's cat. *Rev. Mod. Phys.* **85,** 1103–1114 (2013).
44. Haroche, S. Nobel Lecture: Controlling photons in a box and exploring the quantum to classical boundary. *Rev. Mod. Phys.* **85,** 1083–1102 (2013).

45. Quan, H. T., Liu, Y. X., Sun, C. P. & Nori, F. Quantum thermodynamic cycles and quantum heat engines. *Phys. Rev. E* **76,** 031105 (2007).
46. Abah, O. *et al.* Single-ion heat engine at maximum power. *Phys. Rev. Lett.* **109,** 203006 (2012).
47. Aaronson, S. & Arkhipov, A. in *Proceedings of the 43rd Annual ACM Symposium on Theory of Computing* (eds Fortnow, L. & Vadhan, S.) 333–342 (ACM, 2011).
48. Shen, C. & Duan, L. M. Correcting detection errors in quantum state engineering through data processing. *New J. Phys.* **14,** 053053 (2012).
49. Poschinger, U. *Quantum Optics Experiments in a Microstructured Ion Trap* PhD thesis, Univ. Ulm (2011).
50. Olmschenk, S. *et al.* Manipulation and detection of a trapped Yb^+ hyperfine qubit. *Phys. Rev. A* **76,** 052314 (2007).
51. Zhang, X. *et al.* State-independent experimental tests of quantum contextuality in a three dimensional system. *Phys. Rev. Lett.* **110,** 070401 (2013).

Acknowledgements

We thank C. Jarzynski for careful reading of the manuscript and helpful comments. This work was supported in part by the National Basic Research Program of China Grants 2011CBA00300, 2011CBA00301, the National Natural Science Foundation of China Grants 61073174, 61033001, 61061130540, 11374178, 11375012 and 11105136. K.K. and H.T.Q. acknowledge the recruitment program of Global Youth Experts of China.

Author contributions

S.A., M.U., D.L. and Y.L. developed the experimental system and performed the experiments. Y.L. and S.A. analysed the results. J.Z. developed the adiabatic protocol for the projective measurement. J-N.Z. provided the concrete model for the experiment. J-N.Z., Z-Q.Y. and H.T.Q. provided theoretical support to the project. K.K. supervised the project. All authors contributed to writing the manuscript.

Additional information

Supplementary information is available in the online version of the paper. Reprints and permissions information is available online at www.nature.com/reprints. Correspondence and requests for materials should be addressed to H.T.Q. or K.K.

Competing financial interests

The authors declare no competing financial interests.